

Steady-state interfacial gravity waves with one-dimensional class-III triad resonance

Jiyang Li

*School of Naval Architecture and Ocean Engineering, [Jiangsu University of Science and Technology](#),
Zhenjiang, Jiangsu 212000, PR China
and State Key Laboratory of Ocean Engineering, [Shanghai Jiao Tong University](#), Shanghai 200240, PR China*

Zeng Liu ^{*}


*School of Naval Architecture and Ocean Engineering, [Huazhong University of Science and Technology](#),
Wuhan 430074, PR China
and Hubei Provincial Engineering Research Center of Data Techniques and Supporting Software for Ships,
Wuhan 430074, PR China*

Alistair G. L. Borthwick 

*School of Engineering, [University of Edinburgh](#), Edinburgh EH9 3FB, United Kingdom
and School of Engineering, Computing and Mathematics, [University of Plymouth](#),
Plymouth PL4 8AA, United Kingdom*

Jie Cui

*School of Naval Architecture and Ocean Engineering, [Jiangsu University of Science and Technology](#),
Zhenjiang, Jiangsu 212000, PR China*

Shijun Liao 

*School of Naval Architecture, Ocean and Civil Engineering, [Shanghai Jiao Tong University](#),
Shanghai 200240, PR China*



(Received 11 April 2024; accepted 17 July 2024; published 3 September 2024)

Steady-state interfacial waves exhibiting class-III triad resonance are investigated in a two-layer liquid with a free surface. Two independent linear dispersion relationships related to surface and internal modes exist in the idealized model. One-dimensional class-III triad resonance requires the presence of two short surface wave modes and one long internal wave mode in a copropagating wave system. Convergent series solutions are achieved by the homotopy analysis method (HAM) for steady-state interfacial wave groups involving resonant triads and quartets. Unlike conventional progressive interfacial waves that have small surface amplitude and large interface amplitude, the free surface wave height is far larger than that of the internal interface waves because the resonance interactions comprise multiple surface wave modes and a single internal wave mode. As the upper layer thickness increases, energy from the interface is transported to the free surface, and energy in the whole wave system shifts from shorter to longer resonant triads and quartets. Our results indicate that steady-state interfacial waves with class-III exact and near-resonance interactions among surface and internal wave modes could occur in cases representative of the real ocean.

DOI: [10.1103/PhysRevFluids.9.094801](https://doi.org/10.1103/PhysRevFluids.9.094801)

*Contact author: z_liu@hust.edu.cn

I. INTRODUCTION

Over the past 60 years, research into wave resonance has extended from free surface gravity waves [1] to interfacial gravity waves [2], acoustic-gravity waves [3], Faraday waves [4,5], harbor resonance induced by free surface waves [6,7], etc. Steady-state resonant waves with time-independent amplitude spectra are a special case of the more general unsteady-state resonant waves with time-dependent amplitude spectra. Steady-state resonant wave fields consist of one exact resonant set plus a few nearly resonant components, with the amplitude of each sinusoidal component independent of time.

Phillips [1] proposed that an exactly resonant quartet must be present for unsteady-state resonance to occur in periodic free surface waves, and pointed out that the wave amplitude of the resonant component is proportional to time. Benney [8], Longuet-Higgins [9], and Bretherton [10] further investigated the amplitude equations of a resonant quartet in free surface waves and suggested that an energy-sharing mechanism drove energy transfer with time among the different wave components participating in resonance. Studies of wave resonance were then extended from surface waves to interfacial waves. Two different linear dispersion relationships, corresponding to surface and internal wave modes, exist in the physical idealisation of a two-layer fluid with a free surface. Ball [2] found that a large amount of energy is transferred from the two opposite surface wave modes to an internal wave mode during one-dimensional (1D) class-I triad resonance. Wen [11] used a multiscale perturbation method to investigate the amplitude evolution equations of two opposite internal wave modes and a surface wave mode under 1D class-II triad resonance, and found that the amplitudes of the internal modes grow on a timescale much longer than the period of the surface mode. Alam [12] discovered a new triad resonance (1D class-III) emerged from two copropagating surface wave modes and an internal wave mode, and observed that energy gradually shifts from the primary resonant triad into several nearly resonant components of higher and lower order with time. Choi *et al.* [13] proposed that a 1D class-IV triad resonance condition could occur among two copropagating internal wave modes and a surface wave mode when the density ratio between lower and upper fluid layers exceeds 3. In addition, Choi *et al.* [13] extended the foregoing four types of triad resonance to two-dimensional (2D) waves, and found that the amplitudes of the wave components undergoing resonance interactions all vary periodically with time.

In tackling the problem of steady-state resonance, Liao [14] successfully avoided the singularity caused by an exactly resonant component and obtained steady-state free surface wave solutions in deep water using the homotopy analysis method (HAM) [15,16]. Since then, a large number of theoretical (HAM), numerical, and experimental studies have been conducted on steady-state resonant free surface waves [17–23]. Compared to free surface waves, much less research attention has focused on steady-state resonant interfacial waves for which an exact harmonic resonance condition is satisfied when a surface wave mode and an internal wave mode share the same phase speed and possess an integer ratio of wave lengths. Using a numerical model, Parau and Dias [24] obtained steady-state solutions with near-harmonic resonances, and noted that it is hard to obtain a wave system with exact harmonic resonance. However, Li *et al.* [25] obtained steady-state interfacial wave groups with exact and near-harmonic resonances using HAM, and indicated that energy is transferred from resonant components to primary components as the thickness of the upper fluid layer increases. Besides, Li *et al.* [26] investigated multiple near resonance interactions of steady-state interfacial waves with a rigid-lid upper boundary using a combination of HAM and Galerkin methods, and found that the energy shifts progressively to the sideband of the amplitude spectrum with increasing wave steepness, which effectively broadens the frequency band.

No energy exchange occurs with time among wave components in a steady-state wave system. Steady-state resonance essentially reflects a particular wave energy equilibrium and corresponds to the most basic case of conventional unsteady-state resonance with energy exchange among different wave components over time. For example, let the wave amplitude of an unsteady-state resonant component be $A(t)$, a periodic function of time t . Then, the corresponding wave amplitude of steady-state resonance $A = \text{const}$ represents a special case of $A(t)$. Hence, studies of steady-state resonant

wave systems can provide a way to investigate the characteristics of wave resonance. In the present paper, we define “surface waves” as the free surface, and “interface waves” as the internal interface of the interfacial wave system. Alam [12] reported that interface waves are much longer than surface waves in class-III triad resonance in a copropagating wave system, where the ratio of wave lengths and the direction of propagation both oppose class-I and class-II triad resonances. Hence, class-III resonance is more likely to appear in the real ocean. To the best of our knowledge, steady-state periodic interfacial waves with class-III triad resonance have not been considered to date. Research is therefore needed to reveal the influence of steady-state class-III resonance on the evolution of ocean internal wave spectra. Besides, our approach also provides a different type of free surface and internal waves for wave load estimation and structural design of marine engineering structures, such as ships, submarines, and deep-sea vehicles.

This paper utilizes a HAM-based analytic method to obtain steady-state periodic interfacial gravity waves with 1D class-III triad resonance in a two-layer liquid with a free surface. A parameter study examines the influences of nonlinearity (wave steepness) and upper layer thickness (vertical distance from sea surface to density transition layer) on the amplitudes of wave components, wave spatial profiles, and energy distributions of interfacial waves with multiple resonances. HAM has previously been used to analyze steady-state resonance in free surface waves, interfacial waves, and acoustic-gravity waves [27]. Based on the great freedom in choice of auxiliary linear operators and initial guesses, any singularities and small divisors associated with exact and near resonances are avoided by introducing a piecewise parameter in HAM, enabling convergent series solutions of steady-state interfacial waves to be obtained successfully. The paper makes two main contributions. Convergent series solutions of steady-state periodic interfacial gravity waves with 1D class-III exact and near resonances are obtained via HAM. Resonant interactions are analyzed between multiple surface wave modes and an internal wave mode. Then effects are considered of several environmental parameters on the energy distribution in steady-state resonant interfacial waves.

The paper is structured as follows. Section II describes the mathematical derivation and presents a class-III triad resonance criterion. Section III analyzes the resonance curves and interprets results for multiple exact and near resonances. Section IV lists the main conclusions.

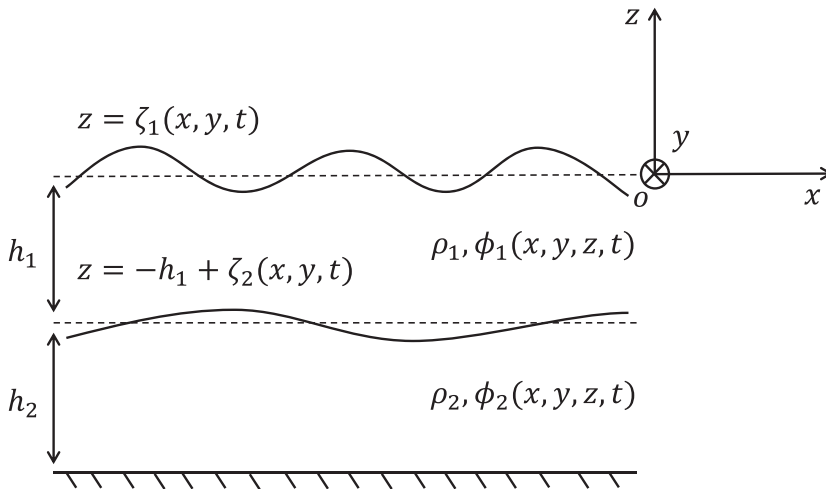


FIG. 1. Sketch showing idealized two-fluid system with related notation.

II. MATHEMATICAL MODEL

A. Governing equations

Consider two inviscid, incompressible, immiscible fluid layers each of constant density that lie one above the other under the influence of gravity. The upper layer, of thickness h_1 , has a free surface. The lower layer thickness is h_2 . The flow is assumed irrotational inside each fluid layer. Figure 1 displays the two-layer fluid system where the density of the upper layer is less than that of the lower layer, $\rho_1 < \rho_2$. Horizontal planes at $z = 0$ and $z = -h_1$ in the Cartesian coordinate system (x, y, z) represent the stationary free surface and the interface between the two fluid layers. The horizontal bed is located at $z = -h_1 - h_2$. Here z is measured vertically upwards. The governing equations for each layer, kinematic boundary condition at the bed, and boundary conditions at the free surface and interface may be written

$$\nabla^2 \phi_1 = 0, \quad -h_1 + \zeta_2 < z < \zeta_1, \quad (1)$$

$$\nabla^2 \phi_2 = 0, \quad -h_1 - h_2 < z < -h_1 + \zeta_2, \quad (2)$$

$$\frac{\partial \phi_2}{\partial z} = 0, \quad z = -h_1 - h_2, \quad (3)$$

$$\frac{\partial^2 \phi_1}{\partial t^2} + g \frac{\partial \phi_1}{\partial z} + \frac{\partial(|\nabla \phi_1|^2)}{\partial t} + \nabla \phi_1 \cdot \nabla \left(\frac{1}{2} |\nabla \phi_1|^2 \right) = 0, \quad \text{at } z = \zeta_1, \quad (4)$$

$$\zeta_1 + \frac{1}{g} \left(\frac{\partial \phi_1}{\partial t} + \frac{1}{2} |\nabla \phi_1|^2 \right) = 0, \quad \text{at } z = \zeta_1, \quad (5)$$

$$\begin{aligned} \frac{\partial^2 \phi_2}{\partial t^2} + g(1 - \Delta) \frac{\partial \phi_2}{\partial z} - \Delta \frac{\partial^2 \phi_1}{\partial t^2} + \frac{\partial(|\nabla \phi_2|^2)}{\partial t} - \Delta \frac{\partial(\frac{1}{2} |\nabla \phi_1|^2)}{\partial t} + \nabla \phi_2 \cdot \nabla \left(\frac{1}{2} |\nabla \phi_2|^2 \right) \\ - \Delta \nabla \phi_2 \cdot \nabla \left(\frac{\partial \phi_1}{\partial t} + \frac{1}{2} |\nabla \phi_1|^2 \right) = 0, \quad \text{at } z = -h_1 + \zeta_2, \end{aligned} \quad (6)$$

$$\begin{aligned} g(1 - \Delta) \frac{\partial(\phi_2 - \phi_1)}{\partial z} + \frac{\partial(\frac{1}{2} |\nabla \phi_2|^2)}{\partial t} + \nabla \phi_2 \cdot \nabla \left(\frac{1}{2} |\nabla \phi_2|^2 \right) - \nabla \phi_1 \cdot \nabla \left(\frac{\partial \phi_2}{\partial t} + \frac{1}{2} |\nabla \phi_2|^2 \right) \\ + \Delta \left[\frac{\partial(\frac{1}{2} |\nabla \phi_1|^2)}{\partial t} + \nabla \phi_1 \cdot \nabla \left(\frac{1}{2} |\nabla \phi_1|^2 \right) - \nabla \phi_2 \cdot \nabla \left(\frac{\partial \phi_1}{\partial t} + \frac{1}{2} |\nabla \phi_1|^2 \right) \right] = 0, \quad \text{at } z = -h_1 + \zeta_2, \end{aligned} \quad (7)$$

$$\zeta_2 - \frac{1}{g(1 - \Delta)} \left[\Delta \left(\frac{\partial \phi_1}{\partial t} + \frac{1}{2} |\nabla \phi_1|^2 \right) - \left(\frac{\partial \phi_2}{\partial t} + \frac{1}{2} |\nabla \phi_2|^2 \right) \right] = 0, \quad \text{at } z = -h_1 + \zeta_2, \quad (8)$$

where $\phi_1(x, y, z, t)$ and $\phi_2(x, y, z, t)$ are the velocity potentials of the upper and lower fluid layers, $z = \zeta_1(x, y, t)$ is the free surface elevation above the mean surface level, $z = -h_1 + \zeta_2(x, y, t)$ is the elevation of the interface between the two layers, g is acceleration due to gravity, t is time, $\Delta = \rho_1/\rho_2$ denotes the density ratio between the upper and lower layers, and $\nabla = \mathbf{e}_x \frac{\partial}{\partial x} + \mathbf{e}_y \frac{\partial}{\partial y} + \mathbf{e}_z \frac{\partial}{\partial z}$ represents the gradient operator. A detailed derivation of the interface deformation conditions (6)–(8) can be found in Appendix of Li *et al.* [25].

Consider a steady-state interfacial wave system with two primary periodic progressive wave components. Let \mathbf{k}_i denote the wave vector and σ_i the actual angular frequency of the i th primary component. Given that the amplitudes of all components in this steady-state system are time-independent, the following transformation is introduced to eliminate the time variable t :

$$\xi_i = \mathbf{k}_i \cdot \mathbf{r} - \sigma_i t, \quad i = 1, 2, \quad (9)$$

where $\mathbf{r} = \mathbf{e}_x x + \mathbf{e}_y y$. The phase of any component in the steady-state wave systems is neglected. We then define

$$\varphi_i(\xi_1, \xi_2, z) = \phi_i(x, y, z, t), \quad \eta_i(\xi_1, \xi_2) = \zeta_i(x, y, t), \quad i = 1, 2, \quad (10)$$

in the new coordinate system (ξ_1, ξ_2, z) . The initial/boundary-value problem (1)–(8) in the original coordinate system (x, y, z, t) is transformed into a boundary-value problem in the coordinate system (ξ_1, ξ_2, z) . Steady-state solutions can be more easily obtained from the boundary-value problem in this new coordinate system without t . Then the governing equations inside the two fluid layers in coordinate system (ξ_1, ξ_2, z) read

$$\widehat{\nabla}^2 \varphi_1 = 0, \quad -h_1 + \eta_2 < z < \eta_1, \quad (11)$$

$$\widehat{\nabla}^2 \varphi_2 = 0, \quad -h_1 - h_2 < z < -h_1 + \eta_2, \quad (12)$$

subject to one kinematic condition and one dynamic boundary condition at the unknown free surface $z = \eta_1$:

$$\mathcal{N}_1[\varphi_1] = \sum_{i=1}^2 \sum_{j=1}^2 \sigma_i \sigma_j \frac{\partial^2 \varphi_1}{\partial \xi_i \partial \xi_j} + g \frac{\partial \varphi_1}{\partial z} - 2 \sum_{i=1}^2 \sigma_i \frac{\partial f_1}{\partial \xi_i} + \widehat{\nabla} \varphi_1 \cdot \widehat{\nabla} f_1 = 0, \quad (13)$$

$$\mathcal{N}_2[\varphi_1, \eta_1] = \eta_1 - \frac{1}{g} \left(\sum_{i=1}^2 \sigma_i \frac{\partial \varphi_1}{\partial \xi_i} - f_1 \right) = 0, \quad (14)$$

three boundary conditions at the unknown interface $z = -h_1 + \eta_2$:

$$\begin{aligned} \mathcal{N}_3[\varphi_1, \varphi_2] &= \sum_{i=1}^2 \sum_{j=1}^2 \sigma_i \sigma_j \frac{\partial^2 \varphi_2}{\partial \xi_i \partial \xi_j} + g(1 - \Delta) \frac{\partial \varphi_2}{\partial z} - \Delta \sum_{i=1}^2 \sum_{j=1}^2 \sigma_i \sigma_j \frac{\partial^2 \varphi_1}{\partial \xi_i \partial \xi_j} + \widehat{\nabla} \varphi_2 \cdot \widehat{\nabla} f_2 \\ &\quad - 2 \sum_{i=1}^2 \sigma_i \frac{\partial f_2}{\partial \xi_i} + \Delta \left(\sum_{i=1}^2 \sigma_i \frac{\partial f_1}{\partial \xi_i} - h_{21} - \widehat{\nabla} \varphi_2 \cdot \widehat{\nabla} f_1 \right) = 0, \end{aligned} \quad (15)$$

$$\begin{aligned} \mathcal{N}_4[\varphi_1, \varphi_2] &= g(1 - \Delta) \frac{\partial(\varphi_2 - \varphi_1)}{\partial z} + \widehat{\nabla}(\varphi_2 - \varphi_1) \cdot \widehat{\nabla} f_2 - h_{12} - \sum_{i=1}^2 \sigma_i \frac{\partial f_2}{\partial \xi_i} \\ &\quad - \Delta \left[\sum_{i=1}^2 \sigma_i \frac{\partial f_1}{\partial \xi_i} + h_{21} + \widehat{\nabla}(\varphi_2 - \varphi_1) \cdot \widehat{\nabla} f_1 \right] = 0, \end{aligned} \quad (16)$$

$$\mathcal{N}_5[\varphi_1, \varphi_2, \eta_2] = \eta_2 - \frac{1}{g(1 - \Delta)} \left[\sum_{i=1}^2 \sigma_i \frac{\partial \varphi_2}{\partial \xi_i} - f_2 - \Delta \left(\sum_{i=1}^2 \sigma_i \frac{\partial \varphi_1}{\partial \xi_i} - f_1 \right) \right] = 0, \quad (17)$$

and a kinematic boundary condition at the bed

$$\frac{\partial \varphi_2}{\partial z} = 0, \quad z = -h_1 - h_2, \quad (18)$$

where \mathcal{N}_i with $i = 1, 2, \dots, 5$ denote nonlinear differential operators, and

$$\widehat{\nabla} = \mathbf{k}_1 \frac{\partial}{\partial \xi_1} + \mathbf{k}_2 \frac{\partial}{\partial \xi_2} + \mathbf{e}_z \frac{\partial}{\partial z}, \quad f_i = \frac{1}{2} |\widehat{\nabla} \varphi_i|^2, \quad i = 1, 2, \quad (19)$$

$$h_{ij} = -\sigma_1 \widehat{\nabla} \varphi_i \cdot \widehat{\nabla} \left(\frac{\partial \varphi_j}{\partial \xi_1} \right) - \sigma_2 \widehat{\nabla} \varphi_i \cdot \widehat{\nabla} \left(\frac{\partial \varphi_j}{\partial \xi_2} \right), \quad i, j = 1, 2. \quad (20)$$

The disturbed free surface and interface elevations, η_1 and η_2 , and the velocity potentials in the upper and lower fluid layers, φ_1 and φ_2 , of the steady-state interfacial wave system can be expressed

as the following series:

$$\eta_1(\xi_1, \xi_2) = \sum_{i=-\infty}^{+\infty} \sum_{j=-\infty}^{+\infty} C_{i,j}^{\eta_1} \cos(i\xi_1 + j\xi_2), \quad (21)$$

$$\eta_2(\xi_1, \xi_2) = \sum_{i=-\infty}^{+\infty} \sum_{j=-\infty}^{+\infty} C_{i,j}^{\eta_2} \cos(i\xi_1 + j\xi_2), \quad (22)$$

$$\varphi_1(\xi_1, \xi_2, z) = \sum_{i=-\infty}^{+\infty} \sum_{j=-\infty}^{+\infty} (C_{i,j}^{\varphi_{1a}} \psi_{i,j}^{1a} + C_{i,j}^{\varphi_{1b}} \psi_{i,j}^{1b}), \quad (23)$$

$$\varphi_2(\xi_1, \xi_2, z) = \sum_{i=-\infty}^{+\infty} \sum_{j=-\infty}^{+\infty} C_{i,j}^{\varphi_2} \psi_{i,j}^2, \quad (24)$$

where

$$\psi_{i,j}^{1a}(\xi_1, \xi_2, z) = \cosh[k_{i,j}(z + h_1)] \sin(i\xi_1 + j\xi_2), \quad (25)$$

$$\psi_{i,j}^{1b}(\xi_1, \xi_2, z) = \sinh[k_{i,j}(z + h_1)] \sin(i\xi_1 + j\xi_2), \quad (26)$$

$$\psi_{i,j}^2(\xi_1, \xi_2, z) = \cosh[k_{i,j}(z + h_1 + h_2)] \sin(i\xi_1 + j\xi_2), \quad (27)$$

$$k_{i,j} = |i\mathbf{k}_1 + j\mathbf{k}_2|. \quad (28)$$

Values of \mathbf{k}_i , σ_i , and h_i with $i = 1, 2$ are required in each case to obtain the unknown constants $C_{i,j}^{\eta_1}$, $C_{i,j}^{\eta_2}$, $C_{i,j}^{\varphi_{1a}}$, $C_{i,j}^{\varphi_{1b}}$, and $C_{i,j}^{\varphi_2}$. Equations (11)–(12) and (18) are automatically satisfied by the series form of η_i , φ_i shown in (21)–(24), and therefore the unknown constants are determined by solving the free surface boundary conditions (13)–(14) at $z = \eta_1$ and the interface boundary conditions (15)–(17) at $z = -h_1 + \eta_2$.

B. Class-III triad resonance condition

Two different linear dispersion relationships (modes) exist in the model (11)–(18). For the surface wave mode, the linear angular frequency is given by

$$\omega_S(k) = \sqrt{gk \frac{CT_1 + CT_2 + \sqrt{(CT_1 + CT_2)^2 - 4(1 - \Delta)(\Delta + CT_1CT_2)}}{2(\Delta + CT_1CT_2)}}, \quad (29)$$

in which $CT_i = \coth(kh_i)$ with $i = 1, 2$. The linear angular frequency of the internal wave mode is

$$\omega_I(k) = \sqrt{gk \frac{CT_1 + CT_2 - \sqrt{(CT_1 + CT_2)^2 - 4(1 - \Delta)(\Delta + CT_1CT_2)}}{2(\Delta + CT_1CT_2)}}. \quad (30)$$

To provide a convenient description of the resonance condition, the linear dispersion relationships (29)–(30) are transformed into the following dimensionless forms:

$$\Omega_S^2(K) = K \frac{CT_1 + CT_2 + \sqrt{(CT_1 + CT_2)^2 - 4(1 - \Delta)(\Delta + CT_1CT_2)}}{2(\Delta + CT_1CT_2)}, \quad (31)$$

$$\Omega_I^2(K) = K \frac{CT_1 + CT_2 - \sqrt{(CT_1 + CT_2)^2 - 4(1 - \Delta)(\Delta + CT_1CT_2)}}{2(\Delta + CT_1CT_2)}, \quad (32)$$

where $h = h_1/h_2$, $K = kh_1$, $\Omega_S = \omega_S \sqrt{h_1/g}$, and $\Omega_I = \omega_I \sqrt{h_1/g}$. Let $k_i = |\mathbf{k}_i|$ with $i = 1, 2$ denote the wave numbers of the two primary components, and k_3 denote the wave number of the exactly resonant component. So-called 1D class-III exact resonance occurs [12,13] when two surface wave

modes $[k_1, \omega_S(k_1)]$ and $[k_3, \omega_S(k_3)]$, and one internal wave mode $[k_2, \omega_I(k_2)]$ all propagate in the same direction, and satisfy the following triad resonance condition:

$$K_3 = K_1 - K_2, \quad \Omega_S(K_3) = \Omega_S(K_1) - \Omega_I(K_2), \quad (33)$$

in which $K_i = k_i h_1$ with $i = 1, 2, 3$. According to Alam [12], the wave length of the internal wave mode is much larger than those of the surface wave modes when exact resonance (33) occurs, causing $K_1 \gg K_2$ and $\Omega_S(K_1) \gg \Omega_I(K_2)$, such that related near resonances may occur when

$$K_{1,n} = K_1 + nK_2, \quad \Omega_S(K_{1,n}) + d\Omega_{1,n} = \Omega_S(K_1) + n\Omega_I(K_2), \quad (34)$$

where $K_{1,n} = k_{1,n} h_1$, $d\Omega_{1,n}$ is a small real number which represents the angular frequency mismatch ($n = \pm 1, \pm 2, \dots$). The near-resonance criteria (34) incorporate resonance interactions between multiple surface wave modes and an internal wave mode, which we call generalized class-III resonances. When $d\Omega = 0$, the near-resonance condition (34) degenerates into exact resonance satisfying (33) when $n = -1$.

The two primary components considered in this paper comprise a surface wave mode $[K_1, \Omega_S(K_1)]$ and an internal wave mode $[K_2, \Omega_I(K_2)]$. After resonant interaction, one exactly or nearly resonant wave component $[K_{1,-1}, \Omega_S(K_{1,-1})]$ appears and several nearly resonant wave components $[K_{1,n}, \Omega_S(K_{1,n})]$ may exist. The foregoing components along with other nonresonant components constitute the whole interfacial wave system.

C. Approach based on HAM

The homotopy analysis method (HAM) is an analytic approximation method for nonlinear partial differential equations, which has been widely applied to problems of free surface gravity wave resonance [14,17–23], acoustic-gravity wave resonance [27], and interfacial gravity wave resonance [25,26]. The general idea behind HAM is to construct a series of continuous deformations between initial guess functions and solutions of nonlinear differential equations. Comprehensive introductions to HAM are given by Liao [15,16]. The basic concept and key details of HAM are described below.

Given that the expressions already obtained for φ_1 (23) and φ_2 (24) automatically satisfy the pair of Laplace equations (11)–(12) and the bottom boundary condition (18), it is sufficient simply to solve the free surface and internal interface conditions (13)–(17). Here we define $q \in [0, 1]$ as an embedding homotopy parameter, $c_0 \neq 0$ as a convergence-control parameter, \mathcal{L}_i with $i = 1, 3, 4$ as the auxiliary linear operators, $\eta_{0,1} = \eta_{0,2} = 0$ as initial guesses for the free surface elevation η_1 , and disturbed interface elevation η_2 , and $\varphi_{0,1}$ and $\varphi_{0,2}$ as initial guesses for the potential functions φ_1 and φ_2 . Then, on the basis of free surface and interface conditions (13)–(17), a parameterized family of equations (called the zeroth-order deformation equations) is constructed as follows:

$$(1 - q)\mathcal{L}_1[\check{\varphi}_1 - \varphi_{0,1}] = qc_0\mathcal{N}_1[\check{\varphi}_1], \quad \text{at } z = \check{\eta}_1, \quad (35)$$

$$(1 - q)\check{\eta}_1 = qc_0\mathcal{N}_2[\check{\varphi}_1, \check{\eta}_1], \quad \text{at } z = \check{\eta}_1, \quad (36)$$

$$(1 - q)\mathcal{L}_3[\check{\varphi}_1 - \varphi_{0,1}, \check{\varphi}_2 - \varphi_{0,2}] = qc_0\mathcal{N}_3[\check{\varphi}_1, \check{\varphi}_2], \quad \text{at } z = -h_1 + \check{\eta}_2, \quad (37)$$

$$(1 - q)\mathcal{L}_4[\check{\varphi}_1 - \varphi_{0,1}, \check{\varphi}_2 - \varphi_{0,2}] = qc_0\mathcal{N}_4[\check{\varphi}_1, \check{\varphi}_2], \quad \text{at } z = -h_1 + \check{\eta}_2, \quad (38)$$

$$(1 - q)\check{\eta}_2 = qc_0\mathcal{N}_5[\check{\varphi}_1, \check{\varphi}_2, \check{\eta}_2], \quad \text{at } z = -h_1 + \check{\eta}_2, \quad (39)$$

where

$$\check{\varphi}_i(\xi_1, \xi_2, z; q) = \sum_{n=0}^{+\infty} \varphi_{n,i} q^n, \quad \varphi_{n,i}(\xi_1, \xi_2, z) = \left. \frac{1}{n!} \frac{\partial^n \check{\varphi}_i}{\partial q^n} \right|_{q=0}, \quad (40)$$

$$\check{\eta}_i(\xi_1, \xi_2; q) = \sum_{n=1}^{+\infty} \eta_{n,i} q^n, \quad \eta_{n,i}(\xi_1, \xi_2) = \left. \frac{1}{n!} \frac{\partial^n \check{\eta}_i}{\partial q^n} \right|_{q=0}, \quad i = 1, 2. \quad (41)$$

Choosing the auxiliary linear operators \mathcal{L}_i with the property $\mathcal{L}_1[0] = \mathcal{L}_3[0, 0] = \mathcal{L}_4[0, 0] = 0$, the following relationships at $q = 0$ are obtained:

$$\check{\varphi}_i(\xi_1, \xi_2, z; 0) = \varphi_{0,i}, \quad \check{\eta}_i(\xi_1, \xi_2; 0) = 0, \quad i = 1, 2. \quad (42)$$

When $q = 1$, Eqs. (35)–(39) are the same as the original Eqs. (13)–(17). Hence,

$$\check{\varphi}_i(\xi_1, \xi_2, z; 1) = \varphi_i, \quad \check{\eta}_i(\xi_1, \xi_2; 1) = \eta_i, \quad i = 1, 2. \quad (43)$$

In short, the zeroth-order deformation equations (35)–(39) define four homotopies

$$\check{\varphi}_i := \varphi_{0,i} \sim \varphi_i, \quad \check{\eta}_i := 0 \sim \eta_i, \quad \text{when } q := 0 \sim 1, \quad i = 1, 2. \quad (44)$$

Setting $q = 1$, the homotopy-series solutions for the free surface elevation η_1 , disturbed interface elevation η_2 , and the velocity potentials in the upper and lower fluid layers φ_1 and φ_2 are expressed (and approximated) by

$$\varphi_i = \sum_{n=0}^{+\infty} \varphi_{n,i} \approx \sum_{n=0}^m \varphi_{n,i}, \quad \eta_i = \sum_{n=1}^{+\infty} \eta_{n,i} \approx \sum_{n=1}^m \eta_{n,i}, \quad i = 1, 2, \quad (45)$$

where the latter terms in the expressions are called m th-order homotopy approximations. The sum indexes of η_1 and η_2 commence from $n = 1$ due to the zero values of initial guesses (i.e., $\eta_{0,1} = \eta_{0,2} = 0$).

1. Solution procedure

Values for $\varphi_{m,i}$ and $\eta_{m,i}$ are obtained by solving the high-order deformation equations step by step:

$$\bar{\mathcal{L}}_1[\varphi_{m,1}] = c_0 \Delta_{m-1,1}^\varphi + \chi_m (S_{m-1,1} - \bar{S}_{m,1}), \quad m \geq 1, \quad (46)$$

$$\bar{\mathcal{L}}_{i+1}[\varphi_{m,1}, \varphi_{m,2}] = c_0 \Delta_{m-1,i}^\varphi + \chi_m (S_{m-1,i} - \bar{S}_{m,i}), \quad i = 2, 3, \quad m \geq 1, \quad (47)$$

$$\eta_{m,i} = c_0 \Delta_{m-1,i}^\eta + \chi_m \eta_{m-1,i}, \quad i = 1, 2, \quad m \geq 1, \quad (48)$$

where the auxiliary linear operators $\bar{\mathcal{L}}_1 = \mathcal{L}_1|_{z=0}$, $\bar{\mathcal{L}}_3 = \mathcal{L}_3|_{z=-h_1}$ and $\bar{\mathcal{L}}_4 = \mathcal{L}_4|_{z=-h_1}$, and define $\chi_1 = 0$ and $\chi_m = 1$ for $m \geq 2$. Up to the m th-order approximation, all terms $\Delta_{m-1,i}^\varphi$, $\bar{S}_{m,i}$, $S_{m-1,i}$, $\Delta_{m-1,i}^\eta$ and $\eta_{m-1,i}$ on the right-hand side of the m th-order deformation equations (46)–(48) are predetermined by $\varphi_{n,i}$ and $\eta_{n,i}$, with $n = 0, 1, 2, \dots, m-1$. Detailed expressions for the high-order deformation equations (46)–(48) are listed in Appendix and in the following section. Values of $\eta_{m,1}$ and $\eta_{m,2}$ are obtained directly from (48), respectively, and $\varphi_{m,1}$ and $\varphi_{m,2}$ are determined by simultaneously solving Eqs. (46)–(47).

If resonance satisfying (34) occurs, we can choose appropriate auxiliary linear operators \mathcal{L}_i and initial guesses in the framework of HAM to avoid encountering the singularity or small denominator caused by each exactly or nearly resonant component so that we obtain convergent series solutions for the steady-state wave system. Similar solution procedures have been applied to cases of multiple near resonances of surface waves [21] and special harmonic resonances between interface and surface waves [25].

2. Choice of auxiliary linear operators

We now consider periodic interfacial waves with class-III resonances (34). First, the following auxiliary linear operators are used to remove all small divisors caused by nearly resonant

components

$$\mathcal{L}_1[\varphi_1] = \omega_1^2 \frac{\partial^2 \varphi_1}{\partial \xi_1^2} + \mu \omega_1 \omega_2 \frac{\partial^2 \varphi_1}{\partial \xi_1 \partial \xi_2} + \omega_2^2 \frac{\partial^2 \varphi_1}{\partial \xi_2^2} + g \frac{\partial \varphi_1}{\partial z}, \quad (49)$$

$$\begin{aligned} \mathcal{L}_3[\varphi_1, \varphi_2] = & \omega_1^2 \frac{\partial^2 \varphi_2}{\partial \xi_1^2} + \mu \omega_1 \omega_2 \frac{\partial^2 \varphi_2}{\partial \xi_1 \partial \xi_2} + \omega_2^2 \frac{\partial^2 \varphi_2}{\partial \xi_2^2} + g(1 - \Delta) \frac{\partial \varphi_2}{\partial z} \\ & - \Delta \left(\omega_1^2 \frac{\partial^2 \varphi_1}{\partial \xi_1^2} + \mu \omega_1 \omega_2 \frac{\partial^2 \varphi_1}{\partial \xi_1 \partial \xi_2} + \omega_2^2 \frac{\partial^2 \varphi_1}{\partial \xi_2^2} \right), \end{aligned} \quad (50)$$

$$\mathcal{L}_4[\varphi_1, \varphi_2] = g(1 - \Delta) \left(\frac{\partial \varphi_2}{\partial z} - \frac{\partial \varphi_1}{\partial z} \right), \quad (51)$$

where $\omega_1 = \omega_S(k_1)$ and $\omega_2 = \omega_I(k_2)$ denote the linear angular frequencies of two primary components, and $\mu = \mu(i, j)$ is a piecewise parameter depending on (i, j) and associated with the component $k_{i,j}$ (28) and defined as

$$\mu(i, j) = \begin{cases} \frac{\omega_S^2(k_{i,j}) - (i^2 \omega_1^2 + j^2 \omega_2^2)}{ij \omega_1 \omega_2}, & (i, j) = (1, n) \\ 2, & \text{else} \end{cases} \quad (52)$$

in which the values of $(1, n)$ correspond to the resonant components described by (34). This piecewise parameter transforms each small denominator into a singularity which is one of the keys to obtaining steady-state solutions. Choice of the auxiliary linear operators (49)–(51) is based on the linear parts of the boundary conditions (13) and (15)–(16). According to the series form (23)–(24), $\varphi_{m,1}$ and $\varphi_{m,2}$ are defined in general form as

$$\varphi_{m,1} = \sum_{i,j} (C_{i,j}^{\varphi_{1a},m} \psi_{i,j}^{1a} + C_{i,j}^{\varphi_{1b},m} \psi_{i,j}^{1b}), \quad \varphi_{m,2} = \sum_{i,j} C_{i,j}^{\varphi_{2,m}} \psi_{i,j}^2. \quad (53)$$

Given that the auxiliary linear operators \mathcal{L}_i , $S_{m,i}$ and $\bar{S}_{m,i}$ are now known, both sides of the m th-order deformation equations (46)–(47) can be simplified to give

$$\bar{\mathcal{L}}_1 \left[\sum_{i,j} (C_{i,j}^{\varphi_{1a},m} \psi_{i,j}^{1a} + C_{i,j}^{\varphi_{1b},m} \psi_{i,j}^{1b}) \right] = \sum_{i,j} R_{i,j}^{1,m} \sin(i\xi_1 + j\xi_2), \quad (54)$$

$$\bar{\mathcal{L}}_3 \left[\sum_{i,j} (C_{i,j}^{\varphi_{1a},m} \psi_{i,j}^{1a} + C_{i,j}^{\varphi_{1b},m} \psi_{i,j}^{1b}), \sum_{i,j} C_{i,j}^{\varphi_{2,m}} \psi_{i,j}^2 \right] = \sum_{i,j} R_{i,j}^{3,m} \sin(i\xi_1 + j\xi_2), \quad (55)$$

$$\bar{\mathcal{L}}_4 \left[\sum_{i,j} (C_{i,j}^{\varphi_{1a},m} \psi_{i,j}^{1a} + C_{i,j}^{\varphi_{1b},m} \psi_{i,j}^{1b}), \sum_{i,j} C_{i,j}^{\varphi_{2,m}} \psi_{i,j}^2 \right] = \sum_{i,j} R_{i,j}^{4,m} \sin(i\xi_1 + j\xi_2), \quad (56)$$

where $C_{i,j}^{\varphi_{1a},m}$, $C_{i,j}^{\varphi_{1b},m}$ and $C_{i,j}^{\varphi_{2,m}}$ are unknown constants to be determined for known $R_{i,j}^{1,m}$, $R_{i,j}^{3,m}$ and $R_{i,j}^{4,m}$. Balancing both sides of (54)–(56), we obtain three linear algebraic equations:

$$\begin{aligned} & gk_{i,j} [C_{i,j}^{\varphi_{1b},m} \cosh(k_{i,j}h_1) + C_{i,j}^{\varphi_{1a},m} \sinh(k_{i,j}h_1)] \\ & - M_{i,j} [C_{i,j}^{\varphi_{1a},m} \cosh(k_{i,j}h_1) + C_{i,j}^{\varphi_{1b},m} \sinh(k_{i,j}h_1)] = R_{i,j}^{1,m}, \end{aligned} \quad (57)$$

$$C_{i,j}^{\varphi_{2,m}} [gk_{i,j}(1 - \Delta) \sinh(k_{i,j}h_2) - M_{i,j} \cosh(k_{i,j}h_2)] + C_{i,j}^{\varphi_{1a},m} \Delta M_{i,j} = R_{i,j}^{3,m}, \quad (58)$$

$$gk_{i,j}(1 - \Delta) [C_{i,j}^{\varphi_{2,m}} \sinh(k_{i,j}h_2) - C_{i,j}^{\varphi_{1b},m}] = R_{i,j}^{4,m}, \quad (59)$$

where

$$M_{i,j} = i^2\omega_1^2 + \mu j\omega_1\omega_2 + j^2\omega_2^2. \quad (60)$$

The solutions for $C_{i,j}^{\varphi_{1a},m}$, $C_{i,j}^{\varphi_{1b},m}$, and $C_{i,j}^{\varphi_2,m}$ are

$$C_{i,j}^{\varphi_{1a},m} = \frac{R_{i,j}^{3,m} + [M_{i,j} \cosh(k_{i,j}h_2) - gk_{i,j}(1 - \Delta) \sinh(k_{i,j}h_2)]C_{i,j}^{\varphi_2,m}}{\Delta M_{i,j}}, \quad (61)$$

$$C_{i,j}^{\varphi_{1b},m} = C_{i,j}^{\varphi_2,m} \sinh(k_{i,j}h_2) - \frac{R_{i,j}^{4,m}}{gk_{i,j}(1 - \Delta)}, \quad (62)$$

$$C_{i,j}^{\varphi_2,m} = D_{i,j} \frac{R_{i,j}^{1,m} + A_{i,j}R_{i,j}^{3,m} + B_{i,j}R_{i,j}^{4,m}}{[\Delta + \coth(k_{i,j}h_1) \coth(k_{i,j}h_2)]\lambda_{i,j}^S \lambda_{i,j}^I}, \quad (63)$$

where

$$A_{i,j} = \frac{1}{\Delta} \left[\cosh(k_{i,j}h_1) - \frac{gk_{i,j} \sinh(k_{i,j}h_1)}{M_{i,j}} \right], \quad (64)$$

$$B_{i,j} = \frac{1}{1 - \Delta} \left[\cosh(k_{i,j}h_1) - \frac{M_{i,j} \sinh(k_{i,j}h_1)}{gk_{i,j}} \right], \quad (65)$$

$$D_{i,j} = -\frac{\Delta M_{i,j}}{\sinh(k_{i,j}h_1) \sinh(k_{i,j}h_2)}, \quad (66)$$

$$\lambda_{i,j}^S = M_{i,j} - \omega_S^2(k_{i,j}), \quad (67)$$

$$\lambda_{i,j}^I = M_{i,j} - \omega_I^2(k_{i,j}). \quad (68)$$

For any nonresonant component $\cos(i\xi_1 + j\xi_2)[(i, j) \neq (1, 0), (0, 1)]$, $\mu = 2$, and $\lambda_{i,j}^S = (i\omega_1 + j\omega_2)^2 - \omega_S^2(k_{i,j})$ and $\lambda_{i,j}^I = (i\omega_1 + j\omega_2)^2 - \omega_I^2(k_{i,j})$ are nontrivial real numbers. $C_{i,j}^{\varphi_2,m}$ is obtained directly from (63) after which $C_{i,j}^{\varphi_{1a},m}$ and $C_{i,j}^{\varphi_{1b},m}$ can be calculated from (61)–(62). For any exactly or nearly resonant component $\cos(\xi_1 + n\xi_2)$, the value of μ is determined by (52) resulting in $\lambda_{1,n}^S = 0$. Each resonant component corresponds to a singularity in the mathematical formulas, and so $C_{1,n}^{\varphi_2,m}$ cannot be obtained from (63). To remove the singularity, the numerator on the right-hand side of (63) is set to zero, such that

$$R_{1,n}^{1,m} + A_{1,n}R_{1,n}^{3,m} + B_{1,n}R_{1,n}^{4,m} = 0, \quad (69)$$

from which the value of $C_{1,n}^{\varphi_2,m-1}$ can be determined. In the same way, $C_{1,n}^{\varphi_2,m}$ is determined by solving the $(m+1)$ th-order Eq. (69). Once the value of $C_{1,n}^{\varphi_2,m}$ has been obtained, $C_{1,n}^{\varphi_{1a},m}$ and $C_{1,n}^{\varphi_{1b},m}$ are determined directly from (61)–(62). The foregoing treatment whereby the singularity is removed is key to obtaining convergent series solutions by HAM for steady-state resonant wave groups. It should be emphasized that $\lambda_{1,0}^S = \lambda_{0,1}^I = 0$ for the two primary components $\cos(\xi_1)$ and $\cos(\xi_2)$. Therefore, the coefficients $C_{i,j}^{\varphi_{1a},m}$, $C_{i,j}^{\varphi_{1b},m}$ and $C_{i,j}^{\varphi_2,m}[(i, j) = (1, 0), (0, 1)]$ are determined in a similar way as if these two primary components are resonant.

3. Choice of initial velocity potentials

On the basis of the linearized solutions of Eqs. (11)–(18), the following initial guesses for velocity potentials are selected:

$$\begin{aligned} \varphi_{0,1} = & \frac{1}{\Delta} \left[\cosh(k_1 h_2) - \frac{gk_1(1-\Delta)}{\omega_1^2} \sinh(k_1 h_2) \right] C_{1,0}^{\varphi_2,0} \psi_{1,0}^{1a} + C_{1,0}^{\varphi_2,0} \sinh(k_1 h_2) \psi_{1,0}^{1b} \\ & + \frac{1}{\Delta} \left[\cosh(k_2 h_2) - \frac{gk_2(1-\Delta)}{\omega_2^2} \sinh(k_2 h_2) \right] C_{0,1}^{\varphi_2,0} \psi_{0,1}^{1a} + C_{0,1}^{\varphi_2,0} \sinh(k_2 h_2) \psi_{0,1}^{1b} \\ & + \sum_{l=1}^L \left\{ \frac{1}{\Delta} \left[\cosh(k_{1,i_l} h_2) - \frac{gk_{1,i_l}(1-\Delta)}{\omega_S^2(k_{1,i_l})} \sinh(k_{1,i_l} h_2) \right] C_{1,i_l}^{\varphi_2,0} \psi_{1,i_l}^{1a} + C_{1,i_l}^{\varphi_2,0} \sinh(k_{1,i_l} h_2) \psi_{1,i_l}^{1b} \right\}, \end{aligned} \quad (70)$$

$$\varphi_{0,2} = C_{1,0}^{\varphi_2,0} \psi_{1,0}^2 + C_{0,1}^{\varphi_2,0} \psi_{0,1}^2 + \sum_{l=1}^L C_{1,i_l}^{\varphi_2,0} \psi_{1,i_l}^2, \quad (71)$$

where L denotes the number of resonant wave components subject to the condition (34), and $(1, i_l)$ corresponds to the resonant component $\cos(\xi_1 + i_l \xi_2)$. Initial guesses for the vertical disturbances of the free surface and interface are $\eta_{0,1} = \eta_{0,2} = 0$. Values of $C_{1,0}^{\varphi_2,0}$, $C_{0,1}^{\varphi_2,0}$ and $C_{1,i_l}^{\varphi_2,0}$ are determined from the nonlinear algebraic equations (69) for $m = 1$. When $m > 1$, unique solutions of $C_{1,0}^{\varphi_2,m-1}$, $C_{0,1}^{\varphi_2,m-1}$, and $C_{1,i_l}^{\varphi_2,m-1}$ are obtained from the linear algebraic equations (69).

Here all singularities and small denominators resulting from exact and near resonances have been avoided by proper choices of auxiliary linear operators and initial guesses. For different wave parameters and environmental conditions, we determine the value of the convergence-control parameter c_0 by minimizing the averaged residual squares with fifth-order approximation [28,29]. Convergent series solutions of the steady-state periodic interfacial waves are therefore achieved when implementing HAM.

III. RESULTS AND DISCUSSION

Until now, studies of class-III triad resonance have all focused on unsteady-state interfacial waves. Alam [12] was the first to discover the class-III resonance condition and obtained copropagating surface and interface waves for a case widely considered in two-layer liquid experiments. Recently, Choi *et al.* [13] extended class-III resonance from 1D to 2D waves. In the present paper, we choose physical parameters similar to those applied previously in unsteady-state wave experiments to obtain 1D steady-state wave solutions.

A. Resonance analysis

We first analyze class-III triad resonance conditions (34). Referring to Alam [12], the wave length of the surface wave mode (31) is much smaller than that of the internal wave mode (32) when exact resonance (33) of the $[K_{1,-1}, \Omega_S(K_{1,-1})]$ component occurs, which is why $K_2 \ll K_1$ and $\Omega_I(K_2) \ll \Omega_S(K_1)$. Hence, the $[K_{1,n}, \Omega_S(K_{1,n})]$ ($n = 1, \pm 2, \pm 3, \dots$) components might be involved in the near resonances (34).

Figure 2 presents exact resonance curves for the $\cos(\xi_1 + n\xi_2)$ ($n = \pm 1, \pm 2, \pm 3$) components that relate the dimensionless wave numbers of primary components K_2 to K_1 . Density ratio Δ and depth ratio h values are partly selected from experimental data for unsteady-state interfacial waves [30,31]. The resonance curves remain closer to each other for primary components with smaller wave numbers. This implies that the longer the wave lengths of primary components, the greater the number of wave components are likely to be involved in resonance. Two groups of exact resonances

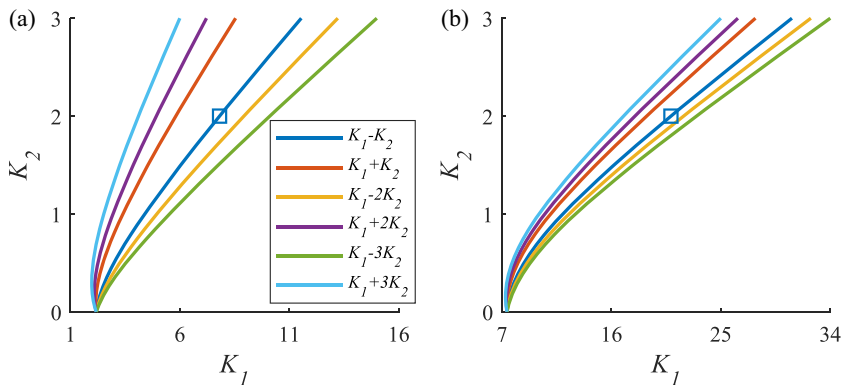


FIG. 2. Each color curve represents the relationship between the dimensionless wave numbers of primary components K_1 and K_2 that satisfy the exact resonance condition (34) ($d\Omega_{1,i_l} = 0$) for the $[K_{1,i_l}, \Omega_S(K_{1,i_l})]$ component: (a) $\Delta = 0.86$ and $h = 0.25$ and (b) $\Delta = 0.95$ and $h = 0.5$. Square symbols indicate exactly resonant cases for the $[K_{1,-1}, \Omega_S(K_{1,-1})]$ component at $K_2 = 2$.

for the $[K_{1,-1}, \Omega_S(K_{1,-1})]$ component marked by square symbols in Fig. 2 are chosen as standard cases here:

$$\Delta = 0.86, \quad h = 0.25, \quad K_2 = k_2 h_1 = 2, \quad K_1 = k_1 h_1 = 7.81302, \quad (72)$$

$$\Delta = 0.95, \quad h = 0.5, \quad K_2 = k_2 h_1 = 2, \quad K_1 = k_1 h_1 = 20.8924, \quad (73)$$

where the larger density and depth ratios cause the wave number ratio K_1/K_2 to increase for fixed $K_2 = 2$. The relative angular frequency mismatch is defined as

$$\nu(1, i_l) = \frac{|d\Omega_{1,i_l}|}{\Omega_S(K_1)}. \quad (74)$$

Taking the exact and several possible nearly resonant components as an example, Table I and Table II list the six resonant components with smallest relative angular frequency mismatches $\log_{10} \nu(1, i_l)$ for the parameters in (72) and (73). The relative angular frequency mismatch increases with the value of $|i_l|$, which indicates that the component $\cos(\xi_1 + i_l \xi_2)$ has smaller resonance probability at larger $|i_l|$. Comparing Table I with Table II, case (73) may contain more nearly resonant components than case (72). For different physical parameters (such as wave steepness, fluid layer depth, and density ratio), these nearly resonant components with small relative angular frequency mismatches might serve as candidates for inclusion in the initial velocity potentials (70)–(71).

TABLE I. Six resonant components $[K_{1,i_l}, \Omega_S(K_{1,i_l})]$ with smallest relative angular frequency mismatches $\log_{10} \nu(1, i_l)$ in case (72) for $|i_l| \leq 20$.

i_l	$\log_{10} \nu(1, i_l)$	i_l	$\log_{10} \nu(1, i_l)$
-1	$-\infty$	2	-1.34
1	-1.78	3	-1.08
-2	-1.58	-3	-0.97

TABLE II. Six resonant components $[K_{1,i_l}, \Omega_S(K_{1,i_l})]$ with smallest relative angular frequency mismatches $\log_{10} \nu(1, i_l)$ in case (73) for $|i_l| \leq 20$.

i_l	$\log_{10} \nu(1, i_l)$	i_l	$\log_{10} \nu(1, i_l)$
-1	$-\infty$	2	-2.18
1	-2.64	-3	-2.07
-2	-2.57	3	-1.90

B. Multiply resonant waves with various nonlinearities

We now consider interfacial waves with an exactly resonant component $\cos(\xi_1 - \xi_2)$ and several nearly resonant components of different nonlinearity. We define the dimensionless angular frequency as the ratio of actual to linear angular frequency $\epsilon = \sigma_1/\omega_1 = \sigma_2/\omega_2$. In general, larger $\epsilon > 1$ corresponds to greater nonlinearity (i.e., wave steepness) for an interfacial wave system filled with copropagating components (see, e.g., [25]). We define the wave steepness of the free surface H_{s1} and internal interface H_{s2} as

$$H_{si} = k_1 \frac{\max[\eta_i(\xi_1, \xi_2)] - \min[\eta_i(\xi_1, \xi_2)]}{2}, \quad \xi_1, \xi_2 \in [0, 2\pi], \quad i = 1, 2. \quad (75)$$

Note that only one group of solutions for $|C_{1,0}^{\varphi_2,0}|$, $|C_{0,1}^{\varphi_2,0}|$ and $|C_{1,i_l}^{\varphi_2,0}|$ in (70)-(71) converges among all solutions of the nonlinear algebraic equations (69) for $m = 1$ in both cases (72) and (73).

Figure 3 displays the relationship between wave steepness (H_{s1} and H_{s2}) and dimensionless angular frequency ϵ for cases (72) and (73). H_{s1} invariably increases with ϵ whereas H_{s2} first increases and then flattens. This occurs because additional surface wave modes appear in the spectrum with rising nonlinearity. Higher dimensionless angular frequency corresponds to greater nonlinearity of the whole wave system, with the majority of nonlinearity concentrated in the surface waves.

Figure 4 shows the variation in dimensionless amplitudes of the six largest wave components $|k_1 C_{1,0}^{\eta_1}|$, $|k_1 C_{0,1}^{\eta_2}|$, $|k_1 C_{1,-1}^{\eta_1}|$, $|k_1 C_{1,1}^{\eta_1}|$, $|k_1 C_{1,-2}^{\eta_1}|$, and $|k_1 C_{1,2}^{\eta_1}|$ with ϵ for the two cases (72) and (73). When ϵ is small, only three wave components exist in the wave system, which is composed of one primary component, $|k_1 C_{1,0}^{\eta_1}|$, and one resonant component, $|k_1 C_{1,-1}^{\eta_1}|$, at the free surface, and one primary component, $|k_1 C_{0,1}^{\eta_2}|$, at the internal interface. As ϵ increases, the amplitudes of all

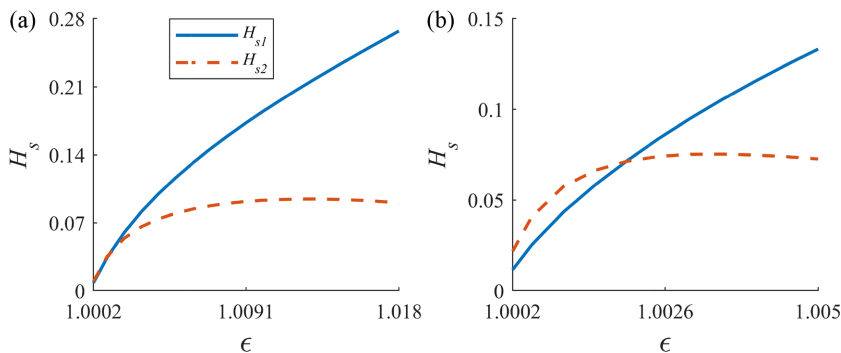


FIG. 3. Variations in free surface wave steepness H_{s1} and internal interface wave steepness H_{s2} for exactly resonant interfacial waves with dimensionless angular frequency ϵ , obtained using parameters in (a) case (72) and (b) case (73).

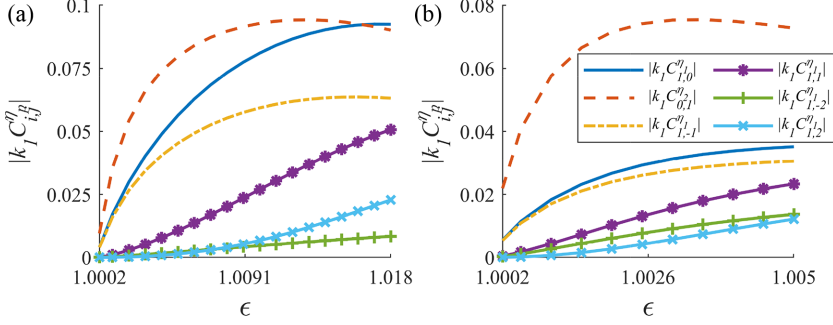


FIG. 4. Variations in wave amplitudes of primary and resonant components $|k_1 C_{i,j}^{\eta}|$ with dimensionless angular frequency ϵ , obtained using the parameters in (a) case (72) and (b) case (73).

six components increase gradually as several components begin to join the resonance interactions, notably the $|k_1 C_{1,1}^{\eta_1}|$ component. Note that for large ϵ , all other components in the interface waves can be neglected except $|k_1 C_{0,1}^{\eta_2}|$, which remains almost constant (decreasing very slightly) with ϵ and is larger than any free surface wave component. The decrease in wave amplitude $|k_1 C_{0,1}^{\eta_2}|$ explains the decrease in wave steepness of the internal interface displayed in Fig. 3. In case (72), the $K_1 + nK_2$ ($n = 0, \pm 1, \pm 2$) components are all smaller than those in case (73), and so the wave lengths of surface wave components in Fig. 4(a) are larger than those in Fig. 4(b). Therefore, the amplitude of each surface wave component in Fig. 4(a) is generally larger than its counterpart in Fig. 4(b) for fixed ϵ . Moreover, the amplitudes of the two primary components $|k_1 C_{1,0}^{\eta_1}|$ and $|k_1 C_{0,1}^{\eta_2}|$ and one exactly resonant component $|k_1 C_{1,-1}^{\eta_1}|$ are all invariably larger than those of the nearly resonant components ($|k_1 C_{1,1}^{\eta_1}|$, $|k_1 C_{1,-2}^{\eta_1}|$ and $|k_1 C_{1,2}^{\eta_1}|$) at any given ϵ . The exactly resonant triad (33) dominates the resonance interactions compared with other near resonances.

According to the series form of the free surface elevation (21) and using the variable transformation (9), the contribution of each surface wave component to the free surface elevation ζ_1 is defined as

$$\zeta_{i,j} = C_{i,j}^{\eta_1} \cos[i(\mathbf{k}_1 \cdot \mathbf{r} - \sigma_1 t) + j(\mathbf{k}_2 \cdot \mathbf{r} - \sigma_2 t)], \quad (76)$$

in which

$$\zeta_1 = \sum_{i=-\infty}^{+\infty} \sum_{j=-\infty}^{+\infty} \zeta_{i,j}. \quad (77)$$

Figures 5(a) and 5(b) present spatial profiles of the free surface $z = \zeta_1$ for different values of dimensionless angular frequency ϵ in cases (72) and (73). As ϵ increases, the free surface crests and troughs both steepen and the free surface wave profiles indicate the presence of wave groups. Figures 5(c) and 5(d) provide spatial profiles of the surface wave components $\zeta_{i,j}$ for cases (72) ($\epsilon = 1.018$) and (73) ($\epsilon = 1.005$). In both cases, all wave components propagate in the same direction and $K_1 \gg K_2$, causing similar wave components $\cos(\xi_1 + n\xi_2)$ to appear at the free surface. In addition, the value of K_1/K_2 in case (72) is smaller than that in case (73), and so the wave groups in Fig. 5(b) possess more crests and troughs than the wave groups in Fig. 5(a) between adjacent wave nodes. The spatial profile of the interface waves is sinusoidal because only one wave component $\cos(\xi_2)$ exists at the interface (see Fig. 4). Hence, the variation in interface wave shape with ϵ is directly captured by $|k_1 C_{0,1}^{\eta_2}|$ in Fig. 4.

Based on linear wave theory and following Tanaka & Wakayama [32], the energy density $E_{i,j}$ of the $\cos(i\xi_1 + j\xi_2)$ component can be defined as

$$E_{i,j}^S = \frac{1}{2} \rho_1 g (C_{i,j}^{\eta_1})^2, \quad E_{i,j}^I = \frac{1}{2} (\rho_2 - \rho_1) g (C_{i,j}^{\eta_2})^2, \quad E_{i,j} = E_{i,j}^S + E_{i,j}^I, \quad (78)$$

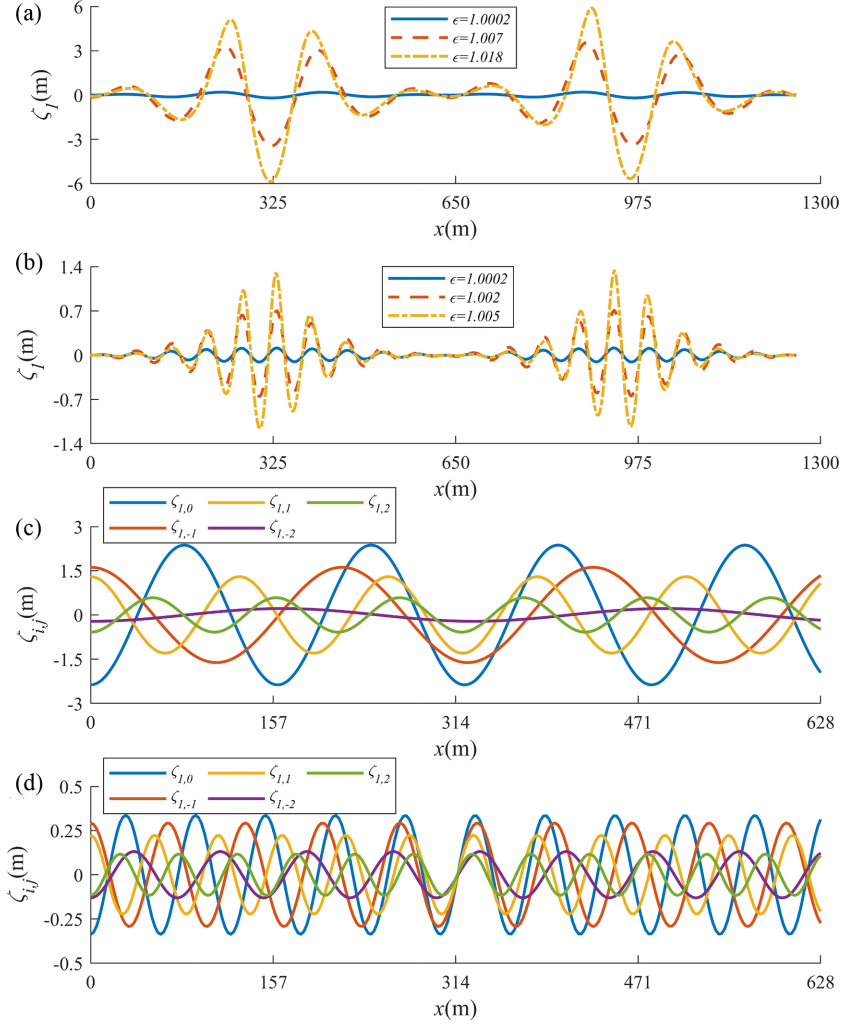


FIG. 5. Spatial profiles of free surface $z = \zeta_1$ at $t = 0$ s for different values of dimensionless angular frequency ϵ obtained using the parameters in case (72) for (a) and case (73) for; and spatial profiles of surface wave components $\zeta_{i,j}$ at $t = 0$ s using parameters in case (72) with $\epsilon = 1.018$ for (c) and case (73) with $\epsilon = 1.005$ for (d).

where $E_{i,j}^S$ and $E_{i,j}^I$ are free surface and internal interface wave energy contributions. Then the total energy densities of surface waves E^S , interface waves E^I , and the whole wave field E are obtained as

$$E^S = \sum_{i=-\infty}^{+\infty} \sum_{j=-\infty}^{+\infty} E_{i,j}^S, \quad E^I = \sum_{i=-\infty}^{+\infty} \sum_{j=-\infty}^{+\infty} E_{i,j}^I, \quad E = E^S + E^I. \quad (79)$$

Figure 6 displays the dependence on ϵ of proportional energy contributions by surface and interface waves, and primary and resonant components over the whole wave field in cases (72) and (73). For interface waves, the proportion of energy related to the unique wave component $E_{0,1}^I$ (equivalent to the proportion of energy carried by the interface waves E^I) directly decreases with ϵ . For surface waves, the proportions of energy carried by the primary component $E_{1,0}^S$ and the

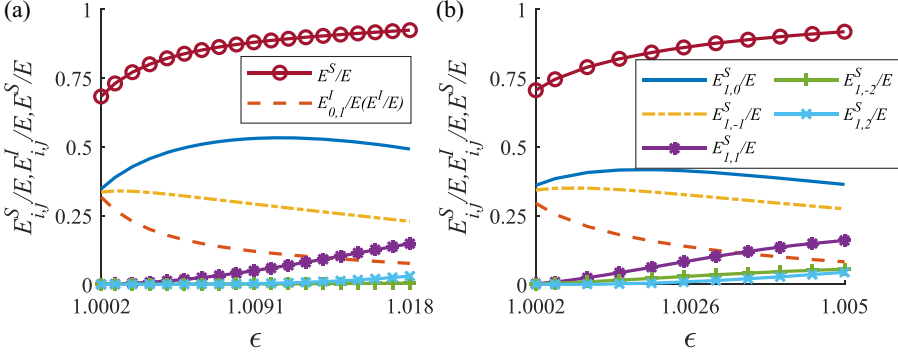


FIG. 6. Variations in proportion of energy carried by surface and interface waves and primary and resonant components with dimensionless angular frequency ϵ , obtained using the parameters in case (72) for (a) and case (73) for (b).

exactly resonant component $E_{1,-1}^S$ both first increase, reach a shallow peak, and then decrease with increasing ϵ , whereas the red proportions of energy carried by the nearly resonant components ($E_{1,1}^S$, $E_{1,-2}^S$, and $E_{1,2}^S$) all increase with ϵ . The exactly resonant triad (33) corresponds to unique resonance interaction for small ϵ . When ϵ is sufficiently large, the exactly resonant triad (33) and the nearly resonant triad (34) for $n = 1$ play important roles in the resonance interactions. In other words, the wave energy spectrum consists of two primary components and one exactly resonant component for small amplitude waves, and contains additional nearly resonant components for finite amplitude waves. The surface waves as a whole carry far more energy than the interface waves. At large $\epsilon > 1.015$ in (72) or $\epsilon > 1.0045$ in (73), the energy proportion of interface waves is less than 9%.

Note that the wave height of the free surface is commonly smaller than that of the internal interface for two-layer interfacial progressive waves with similar densities, as reported by Thorpe [33]. However, as shown in Figs. 3 and 6, the wave height and energy of the free surface are much larger than those of the internal interface for moderately nonlinear cases due to multiple resonance interactions (34).

C. Effect of upper layer thickness on finite amplitude waves

This section examines the influence of the upper liquid layer thickness on finite amplitude interfacial waves with exact and near resonances. The following invariant parameters are selected from the $K_{1,-1}$ exact resonance cases (72) and (73) with fixed values of dimensionless angular frequency ϵ ,

$$\Delta = 0.86, \quad k_1 h_2 = 31.25, \quad k_2 h_2 = 8, \quad \epsilon = 1.012, \quad (80)$$

$$\Delta = 0.95, \quad k_1 h_2 = 41.78, \quad k_2 h_2 = 4, \quad \epsilon = 1.0035, \quad (81)$$

for different values of upper liquid layer thickness h_1 .

Figure 7 presents dimensionless amplitudes of the six largest wave components $|k_1 C_{1,0}^{\eta_1}|$, $|k_1 C_{0,1}^{\eta_2}|$, $|k_1 C_{1,-1}^{\eta_1}|$, $|k_1 C_{1,1}^{\eta_1}|$, $|k_1 C_{1,-2}^{\eta_1}|$, and $|k_1 C_{1,2}^{\eta_1}|$ with increased dimensionless upper layer depth $k_2 h_1$ for cases (80) and (81). When $k_2 h_1$ is small, $|k_1 C_{1,1}^{\eta_1}|$, $|k_1 C_{1,0}^{\eta_1}|$, and $|k_1 C_{1,2}^{\eta_1}|$ are dominant components of the surface waves. As $k_2 h_1$ increases, the wave amplitudes of the three components $|k_1 C_{1,0}^{\eta_1}|$, $|k_1 C_{1,-1}^{\eta_1}|$, and $|k_1 C_{1,-2}^{\eta_1}|$ increase, the component $|k_1 C_{1,2}^{\eta_1}|$ decreases, and the component $|k_1 C_{1,1}^{\eta_1}|$ first increases a little and then decreases gradually. For large $k_2 h_1$, $|k_1 C_{1,0}^{\eta_1}|$, $|k_1 C_{1,-1}^{\eta_1}|$ and $|k_1 C_{1,1}^{\eta_1}|$ dominate the free surface motion. For interface waves, the sole component $|k_1 C_{0,1}^{\eta_2}|$ increases,

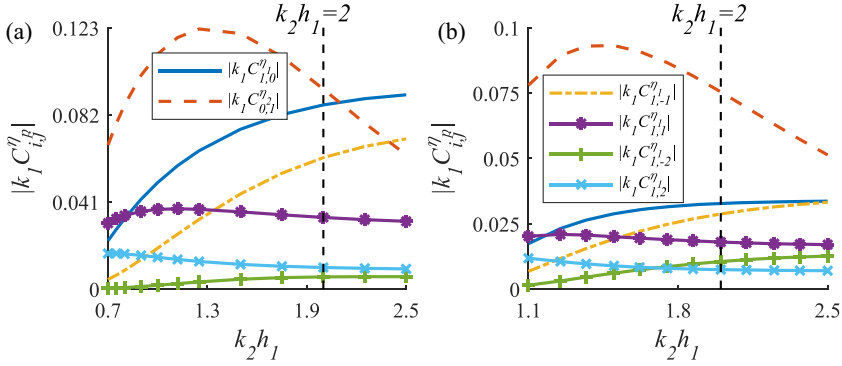


FIG. 7. Variations in wave amplitudes of primary and resonant components $|k_1 C_{i,j}^{\eta}|$ with dimensionless upper layer thickness $k_2 h_1$, obtained using the parameters in case (80) for (a) and case (81) for (b). Black dotted lines $k_2 h_1 = 2$ represent exact resonances for the $[K_{1,-1}, \Omega_S(K_{1,-1})]$ component.

reaches a peak, and then decreases with increasing $k_2 h_1$; the peak occurs at $k_2 h_1 = 1.25$ for case (80) and $k_2 h_1 = 1.5$ for case (81). The resonant triad (34) with $n = 1$ is the most important resonance interaction in a shallow upper liquid layer. For a deep upper fluid layer, the dominant resonant triad (34) corresponds to $n = -1$. This implies that the dominant resonant component might change with upper layer thickness. The wave lengths of surface wave components in Fig. 7(a) are larger than those in Fig. 7(b), and so the amplitudes of the surface wave components in Fig. 7(a) are larger than their counterparts in Fig. 7(b) for fixed $k_2 h_1$.

Figure 8 displays spatial profiles of the free surface elevation $z = \zeta_1$ with different values of dimensionless upper layer thickness $k_2 h_1$ for cases (80) and (81). Crests and troughs of the surface waves steepen with $k_2 h_1$, whereas those of the interface waves first steepen and then flatten with

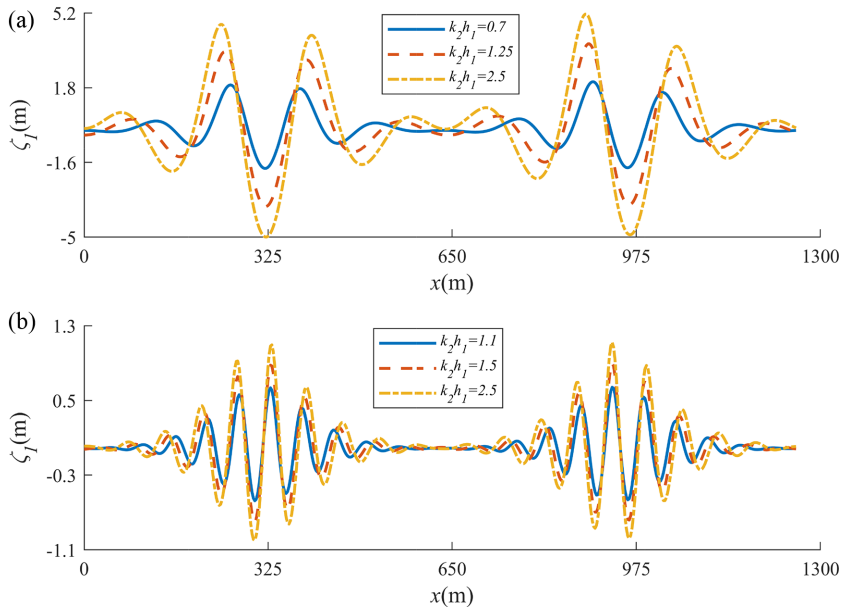


FIG. 8. Spatial profiles of free surface $z = \zeta_1$ at $t = 0$ s for different values of dimensionless upper layer thickness $k_2 h_1$ obtained using the parameters in case (80) for (a) and case (81) for (b).

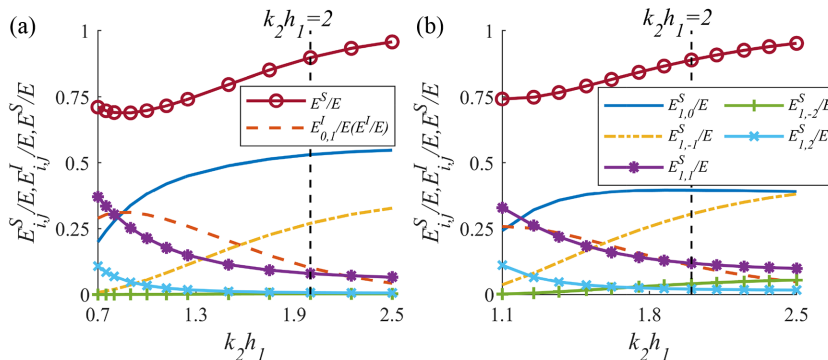


FIG. 9. Variations in proportion of energy carried by surface and interface waves and primary and resonant components with dimensionless upper layer depth thickness $k_2 h_1$, obtained using the parameters in case (80) for case (a) and (81) for (b). Black dotted lines $k_2 h_1 = 2$ represent exact resonances for the $[K_{1,-1}, \Omega_S(K_{1,-1})]$ component.

increasing $k_2 h_1$ as shown in Fig. 7 for the $|k_1 C_{0,1}^{\eta_2}|$ component. A critical upper liquid layer exists for which the maximum interface waves can occur.

Figure 9 shows the variations with increasing $k_2 h_1$ of proportional energy contributions by surface and interface waves and primary and resonant components for cases (80) and (81). For interface waves, as $k_2 h_1$ rises, the energy density of the sole wave component $E_{0,1}^I$ (equivalent to the proportion of the interface waves E^I) first increases a little, peaks, and then decreases rapidly for case (80) [see Fig. 9(a)] and decreases continuously in case (81) [see Fig. 9(b)]. For the surface waves, the proportions of energy carried by $E_{1,1}^S$ and $E_{1,2}^S$ resonant components both decrease, those by $E_{1,-1}^S$ and $E_{1,-2}^S$ both increase, and that by the primary component $E_{1,0}^S$ first increases rapidly and then saturates with increasing $k_2 h_1$. The wave energy has four main components $E_{1,0}^S$, $E_{0,1}^I$, $E_{1,1}^S$, and $E_{1,2}^S$, corresponding to the resonant triad (34) for $n = 1$ and the resonant quartet (34) for $n = 2$ when the upper layer thickness is small. For a deep upper layer, the resonant triad (34) for $n = -1$ is the dominant resonant interaction. Moreover, the resonant quartet (34) for $n = -2$ cannot be neglected. The wave numbers of all primary and resonant components in the surface waves satisfy

$$K_1 - 2K_2 < K_1 - K_2 < K_1 < K_1 + K_2 < K_1 + 2K_2. \quad (82)$$

This indicates that the majority of wave energy is carried by the surface waves, especially when the upper layer is deep. As the thickness of the upper fluid layer increases, energy is transferred from the interface waves to the surface waves. Within the surface waves, energy is transferred from the shorter resonant components $K_{1,1}$ and $K_{1,2}$ to the longer primary and resonant components $K_{1,0}$, $K_{1,-1}$, and $K_{1,-2}$.

IV. CONCLUDING REMARKS

This paper has investigated steady-state periodic interfacial waves with 1D class-III triad exact and near resonances. The interfacial waves propagate in a two-layer fluid with a free surface, where the density ratios are the same as those used in previous experimental studies of unsteady-state interfacial waves [30,31]. The HAM, an analytic approximation method, has been applied to avoid singularities and small denominators that would otherwise be caused by exact and near resonances. Convergent series solutions have been achieved, and the influences of different physical parameters on steady-state resonant interfacial waves have been interpreted.

For interfacial waves with class-III exact and near resonances, wave groups obviously exist at the free surface. As nonlinearity increases, the original exactly resonant triad condition (33) controls resonance interactions, even though several components gradually join the near-resonance

interactions. Unlike conventional progressive interfacial waves with small amplitude free surface and large amplitude internal interface [33], when nonlinearity is moderate, the wave steepness and energy of the free surface are much larger than those of the internal interface; this occurs because the resonance interactions contain multiple surface wave modes and only one internal wave mode.

For finite amplitude interfacial waves with multiple resonances, as the upper layer depth increases, the core resonance interaction changes from resonant triad (34) for $n = 1$ to resonant triad (34) for $n = -1$. This implies that the upper layer thickness exerts great influence on resonance interactions. Wave energy flows from the interface to the free surface with increased upper layer thickness. For any upper layer thickness, the free surface carries most of the energy in the whole interfacial wave system. For wave components at the free surface, energy transport for varying upper layer depth is likely to be related to the wave lengths of all components involved in resonance. As the upper layer thickness increases, wave energy at the free surface is primarily transferred from shorter wave components in the resonant triad $K_{1,1}$ and quartet $K_{1,2}$ to longer components in the resonant triad $K_{1,-1}$ and quartet $K_{1,-2}$. In addition, increased thickness of the upper fluid layer corresponds to steeper free surface crests and troughs. Meanwhile, the interface first steepens, peaks, and then flattens with increasing upper layer thickness.

In this work, we have analyzed 1D class-III resonances of long-crested steady-state interfacial waves. This has led to the discovery of a type of free surface and internal waves whose potential existence is important for wave load analysis and the structural design of ships, submarines, and deep-sea vehicles. In future work, we intend to investigate other types of steady-state resonance that may arise among surface and internal wave modes. We also intend to carry out physical experiments concerning the complicated interfacial waves identified in this paper when suitable wave tank facilities become available. We will also consider the unsteady-state resonance between interface and surface waves to further analyze, and hence predict, the energy transfer phenomenon.

ACKNOWLEDGMENTS

This work was partly supported by the National Natural Science Foundation of China (Approvals No. 12202166, No. 12072126, No. 52271319), State Key Laboratory of Ocean Engineering (Shanghai Jiao Tong University) (Grants No. GKZD010089 and No. GKZD010087), Natural Science Foundation of Jiangsu Province of China (Approval No. BK20231525), and the Doctor of Innovation and Entrepreneurship Project of Jiangsu Province, China (Approval No. JSSCBS20221267).

The authors report no conflicts of interest.

APPENDIX: HIGH-ORDER DEFORMATION EQUATIONS IN HAM

Substituting the series (40)–(41) into the zeroth-order deformation equations (35)–(39), and then equating each like power of q , we obtain the following five linear partial differential equations (called high-order deformation equations):

$$\bar{\mathcal{L}}_1[\varphi_{m,1}] = c_0 \Delta_{m-1,1}^\varphi + \chi_m (S_{m-1,1} - \bar{S}_{m,1}), \quad m \geq 1, \quad (\text{A1})$$

$$\bar{\mathcal{L}}_{i+1}[\varphi_{m,1}, \varphi_{m,2}] = c_0 \Delta_{m-1,i}^\varphi + \chi_m (S_{m-1,i} - \bar{S}_{m,i}), \quad i = 2, 3, \quad m \geq 1, \quad (\text{A2})$$

$$\eta_{m,i} = c_0 \Delta_{m-1,i}^\eta + \chi_m \eta_{m-1,i}, \quad i = 1, 2, \quad m \geq 1, \quad (\text{A3})$$

defining $\bar{\mathcal{L}}_1 = \mathcal{L}_1|_{z=0}$, $\bar{\mathcal{L}}_3 = \mathcal{L}_3|_{z=-h_1}$, $\bar{\mathcal{L}}_4 = \mathcal{L}_4|_{z=-h_1}$, $\chi_1 = 0$ and $\chi_m = 1$ for $m \geq 2$, and where

$$\Delta_{m,1}^\varphi = \sigma_1^2 \bar{\phi}_m^{2,0,1,1} + 2\sigma_1 \sigma_2 \bar{\phi}_m^{1,1,1,1} + \sigma_2^2 \bar{\phi}_m^{0,2,1,1} + g \bar{\phi}_{z,m}^{0,0,1,1} + \Lambda_{m,1}^{1,1,1} - 2(\sigma_1 \Gamma_{m,1}^{1,1} + \sigma_2 \Gamma_{m,2}^{1,1}), \quad (\text{A4})$$

$$\begin{aligned} \Delta_{m,2}^\varphi &= \sigma_1^2 \bar{\phi}_m^{2,0,2,2} + 2\sigma_1 \sigma_2 \bar{\phi}_m^{1,1,2,2} + \sigma_2^2 \bar{\phi}_m^{0,2,2,2} + g(1 - \Delta) \bar{\phi}_{z,m}^{0,0,2,2} \\ &\quad - \Delta(\sigma_1^2 \bar{\phi}_m^{2,0,1,2} + 2\sigma_1 \sigma_2 \bar{\phi}_m^{1,1,1,2} + \sigma_2^2 \bar{\phi}_m^{0,2,1,2}) + \Lambda_{m,1}^{2,2,2} \\ &\quad - 2(\sigma_1 \Gamma_{m,1}^{2,2} + \sigma_2 \Gamma_{m,2}^{2,2}) + \Delta(\sigma_1 \Gamma_{m,1}^{1,2} + \sigma_2 \Gamma_{m,2}^{1,2} - \Lambda_{m,2}^{2,1,2} - \Lambda_{m,1}^{2,1,2}), \end{aligned} \quad (\text{A5})$$

$$\Delta_{m,3}^\varphi = g(1 - \Delta)(\bar{\phi}_{z,m}^{0,0,2,2} - \bar{\phi}_{z,m}^{0,0,1,2}) - \sigma_1 \Gamma_{m,1}^{2,2} - \sigma_2 \Gamma_{m,2}^{2,2} + \Lambda_{m,1}^{2,2,2} - \Lambda_{m,2}^{1,2,2} - \Lambda_{m,1}^{1,2,2} + \Delta(\Lambda_{m,1}^{1,1,2} - \Lambda_{m,2}^{2,1,2} - \Lambda_{m,1}^{2,1,2} - \sigma_1 \Gamma_{m,1}^{1,2} - \sigma_2 \Gamma_{m,2}^{1,2}), \quad (\text{A6})$$

$$\Delta_{m,1}^\eta = \eta_{m,1} - \frac{1}{g}(\sigma_1 \bar{\phi}_m^{1,0,1,1} + \sigma_2 \bar{\phi}_m^{0,1,1,1} - \Gamma_{m,0}^{1,1}), \quad (\text{A7})$$

$$\Delta_{m,2}^\eta = \eta_{m,2} + \frac{1}{g(1 - \Delta)}[\Gamma_{m,0}^{2,2} - \sigma_1 \bar{\phi}_m^{1,0,2,2} - \sigma_2 \bar{\phi}_m^{0,1,2,2} + \Delta(\sigma_1 \bar{\phi}_m^{1,0,1,2} + \sigma_2 \bar{\phi}_m^{0,1,1,2} - \Gamma_{m,0}^{1,2})], \quad (\text{A8})$$

$$S_{m,1} = \omega_1^2 \beta_{2,0,1,1}^{m,0} + \mu \omega_1 \omega_2 \beta_{1,1,1,1}^{m,0} + \omega_2^2 \beta_{0,2,1,1}^{m,0} + g \gamma_{0,0,1,1}^{m,0} + \bar{S}_{m,1}, \quad (\text{A9})$$

$$\bar{S}_{m,1} = \sum_{n=1}^{m-1} (\omega_1^2 \beta_{2,0,1,1}^{m-n,n} + \mu \omega_1 \omega_2 \beta_{1,1,1,1}^{m-n,n} + \omega_2^2 \beta_{0,2,1,1}^{m-n,n} + g \gamma_{0,0,1,1}^{m-n,n}), \quad (\text{A10})$$

$$S_{m,2} = \omega_1^2 \beta_{2,0,2,2}^{m,0} + \mu \omega_1 \omega_2 \beta_{1,1,2,2}^{m,0} + \omega_2^2 \beta_{0,2,2,2}^{m,0} + g(1 - \Delta) \gamma_{0,0,2,2}^{m,0} - \Delta(\omega_1^2 \beta_{2,0,1,2}^{m,0} + \mu \omega_1 \omega_2 \beta_{1,1,1,2}^{m,0} + \omega_2^2 \beta_{0,2,1,2}^{m,0}) + \bar{S}_{m,2}, \quad (\text{A11})$$

$$\bar{S}_{m,2} = \sum_{n=1}^{m-1} [\omega_1^2 \beta_{2,0,2,2}^{m-n,n} + \mu \omega_1 \omega_2 \beta_{1,1,2,2}^{m-n,n} + \omega_2^2 \beta_{0,2,2,2}^{m-n,n} + g(1 - \Delta) \gamma_{0,0,2,2}^{m-n,n} - \Delta(\omega_1^2 \beta_{2,0,1,2}^{m-n,n} + \mu \omega_1 \omega_2 \beta_{1,1,1,2}^{m-n,n} + \omega_2^2 \beta_{0,2,1,2}^{m-n,n})], \quad (\text{A12})$$

$$S_{m,3} = g(1 - \Delta)(\gamma_{0,0,2,2}^{m,0} - \gamma_{0,0,1,2}^{m,0}) + \bar{S}_{m,3}, \quad (\text{A13})$$

$$\bar{S}_{m,3} = \sum_{n=1}^{m-1} [g(1 - \Delta)(\gamma_{0,0,2,2}^{m-n,n} - \gamma_{0,0,1,2}^{m-n,n})], \quad (\text{A14})$$

in which

$$\Gamma_{m,0}^{\bar{k},p} = \sum_{n=0}^m \left(\frac{k_1^2}{2} \bar{\phi}_n^{1,0,\bar{k},p} \bar{\phi}_{m-n}^{1,0,\bar{k},p} + \mathbf{k}_1 \cdot \mathbf{k}_2 \bar{\phi}_n^{1,0,\bar{k},p} \bar{\phi}_{m-n}^{0,1,\bar{k},p} + \frac{k_2^2}{2} \bar{\phi}_n^{0,1,\bar{k},p} \bar{\phi}_{m-n}^{0,1,\bar{k},p} + \frac{1}{2} \bar{\phi}_{z,n}^{0,0,\bar{k},p} \bar{\phi}_{z,m-n}^{0,0,\bar{k},p} \right), \quad \bar{k}, p = 1, 2, \quad (\text{A15})$$

$$\Gamma_{m,1}^{\bar{k},p} = \sum_{n=0}^m [k_1^2 \bar{\phi}_n^{1,0,\bar{k},p} \bar{\phi}_{m-n}^{2,0,\bar{k},p} + \mathbf{k}_1 \cdot \mathbf{k}_2 (\bar{\phi}_n^{1,0,\bar{k},p} \bar{\phi}_{m-n}^{1,1,\bar{k},p} + \bar{\phi}_n^{2,0,\bar{k},p} \bar{\phi}_{m-n}^{0,1,\bar{k},p}) + k_2^2 \bar{\phi}_n^{0,1,\bar{k},p} \bar{\phi}_{m-n}^{1,1,\bar{k},p} + \bar{\phi}_{z,n}^{0,0,\bar{k},p} \bar{\phi}_{z,m-n}^{1,0,\bar{k},p}], \quad \bar{k}, p = 1, 2, \quad (\text{A16})$$

$$\Gamma_{m,2}^{\bar{k},p} = \sum_{n=0}^m [k_1^2 \bar{\phi}_n^{1,0,\bar{k},p} \bar{\phi}_{m-n}^{1,1,\bar{k},p} + \mathbf{k}_1 \cdot \mathbf{k}_2 (\bar{\phi}_n^{1,0,\bar{k},p} \bar{\phi}_{m-n}^{0,2,\bar{k},p} + \bar{\phi}_n^{0,1,\bar{k},p} \bar{\phi}_{m-n}^{1,1,\bar{k},p}) + k_2^2 \bar{\phi}_n^{0,1,\bar{k},p} \bar{\phi}_{m-n}^{0,2,\bar{k},p} + \bar{\phi}_{z,n}^{0,0,\bar{k},p} \bar{\phi}_{z,m-n}^{0,1,\bar{k},p}], \quad \bar{k}, p = 1, 2, \quad (\text{A17})$$

$$\Gamma_{m,3}^{\bar{k},p} = \sum_{n=0}^m [k_1^2 \bar{\phi}_n^{1,0,\bar{k},p} \bar{\phi}_{z,m-n}^{1,0,\bar{k},p} + \mathbf{k}_1 \cdot \mathbf{k}_2 (\bar{\phi}_n^{1,0,\bar{k},p} \bar{\phi}_{z,m-n}^{0,1,\bar{k},p} + \bar{\phi}_n^{0,1,\bar{k},p} \bar{\phi}_{z,m-n}^{1,0,\bar{k},p}) + k_2^2 \bar{\phi}_n^{0,1,\bar{k},p} \bar{\phi}_{z,m-n}^{0,1,\bar{k},p} + \bar{\phi}_{z,n}^{0,0,\bar{k},p} \bar{\phi}_{z,m-n}^{0,0,\bar{k},p}], \quad \bar{k}, p = 1, 2, \quad (\text{A18})$$

$$\Lambda_{m,1}^{i,j,p} = \sum_{n=0}^m [k_1^2 \bar{\phi}_n^{1,0,i,p} \Gamma_{m-n,1}^{j,p} + \mathbf{k}_1 \cdot \mathbf{k}_2 (\bar{\phi}_n^{1,0,i,p} \Gamma_{m-n,2}^{j,p} + \bar{\phi}_n^{0,1,i,p} \Gamma_{m-n,1}^{j,p}) + k_2^2 \bar{\phi}_n^{0,1,i,p} \Gamma_{m-n,2}^{j,p} + \bar{\phi}_{z,n}^{0,0,i,p} \Gamma_{m-n,3}^{j,p}], \quad i, j, p = 1, 2, \quad (\text{A19})$$

$$\Lambda_{m,2}^{i,j,p} = -\sigma_1 \sum_{n=0}^m [k_1^2 \bar{\phi}_n^{1,0,i,p} \bar{\phi}_{m-n}^{2,0,j,p} + \mathbf{k}_1 \cdot \mathbf{k}_2 (\bar{\phi}_n^{1,0,i,p} \bar{\phi}_{m-n}^{1,1,j,p} + \bar{\phi}_n^{0,1,i,p} \bar{\phi}_{m-n}^{2,0,j,p}) + k_2^2 \bar{\phi}_n^{0,1,i,p} \bar{\phi}_{m-n}^{1,1,j,p} + \bar{\phi}_{z,n}^{0,0,i,p} \bar{\phi}_{z,m-n}^{1,0,j,p}] - \sigma_2 \sum_{n=0}^m [k_1^2 \bar{\phi}_n^{1,0,i,p} \bar{\phi}_{m-n}^{1,1,j,p} + k_2^2 \bar{\phi}_n^{0,1,i,p} \bar{\phi}_{m-n}^{0,2,j,p} + \bar{\phi}_{z,n}^{0,0,i,p} \bar{\phi}_{z,m-n}^{0,1,j,p} + \mathbf{k}_1 \cdot \mathbf{k}_2 (\bar{\phi}_n^{1,0,i,p} \bar{\phi}_{m-n}^{0,2,j,p} + \bar{\phi}_n^{0,1,i,p} \bar{\phi}_{m-n}^{1,1,j,p})], \quad i, j, p = 1, 2, \quad (\text{A20})$$

$$\mu_{m,n,p} = \begin{cases} \eta_{n,p}, & m = 1, \quad n \geq 1, \\ \sum_{i=m-1}^{n-1} \mu_{m-1,i,p} \eta_{n-i,p}, & m \geq 2, \quad n \geq m, \end{cases} \quad (\text{A21})$$

$$\psi_{i,j,\bar{k},1}^{n,m} = \frac{\partial^{i+j}}{\partial \xi_i^i \partial \xi_j^j} \left(\frac{1}{m!} \frac{\partial^m \varphi_{n,\bar{k}}}{\partial z^m} \Big|_{z=0} \right), \quad \bar{k} = 1, 2, \quad (\text{A22})$$

$$\psi_{i,j,\bar{k},2}^{n,m} = \frac{\partial^{i+j}}{\partial \xi_i^i \partial \xi_j^j} \left(\frac{1}{m!} \frac{\partial^m \varphi_{n,\bar{k}}}{\partial z^m} \Big|_{z=-h_1} \right), \quad \bar{k} = 1, 2, \quad (\text{A23})$$

$$\beta_{i,j,\bar{k},p}^{n,m} = \begin{cases} \psi_{i,j,\bar{k},p}^{n,0}, & m = 0, \\ \sum_{s=1}^m \psi_{i,j,\bar{k},p}^{n,s} \mu_{s,m,p}, & m \geq 1, \end{cases} \quad (\text{A24})$$

$$\gamma_{i,j,\bar{k},p}^{n,m} = \begin{cases} \psi_{i,j,\bar{k},p}^{n,1}, & m = 0, \\ \sum_{s=1}^m (s+1) \psi_{i,j,\bar{k},p}^{n,s+1} \mu_{s,m,p}, & m \geq 1, \end{cases} \quad (\text{A25})$$

$$\delta_{i,j,\bar{k},p}^{n,m} = \begin{cases} 2\psi_{i,j,\bar{k},p}^{n,2}, & m = 0, \\ \sum_{s=1}^m (s+1)(s+2) \psi_{i,j,\bar{k},p}^{n,s+2} \mu_{s,m,p}, & m \geq 1, \end{cases} \quad (\text{A26})$$

$$\bar{\phi}_n^{i,j,\bar{k},p} = \sum_{m=0}^n \beta_{i,j,\bar{k},p}^{n-m,m}, \quad \bar{\phi}_{z,n}^{i,j,\bar{k},p} = \sum_{m=0}^n \gamma_{i,j,\bar{k},p}^{n-m,m}, \quad \bar{\phi}_{zz,n}^{i,j,\bar{k},p} = \sum_{m=0}^n \delta_{i,j,\bar{k},p}^{n-m,m}. \quad (\text{A27})$$

Detailed expressions for \mathcal{L}_i , $S_{m-1,i}$, and $\bar{S}_{m,i}$ are given in Sec. II C 2.

-
- [1] O. M. Phillips, On the dynamics of unsteady gravity waves of finite amplitude. Part 1. The elementary interactions, *J. Fluid Mech.* **9**, 193 (1960).
 [2] F. K. Ball, Energy transfer between external and internal gravity waves, *J. Fluid Mech.* **19**, 465 (1964).
 [3] U. Kadri and M. Stiassnie, Generation of an acoustic-gravity wave by two gravity waves, and their subsequent mutual interaction, *J. Fluid Mech.* **735**, R6 (2013).
 [4] X. C. Li, X. M. Li, and S. J. Liao, Pattern transition of two-dimensional Faraday waves at an extremely shallow depth, *Sci. China Phys. Mech. Astron.* **59**, 114712 (2016).

- [5] X. C. Li, J. Li, X. M. Li, S. J. Liao, and C. H. Chen, Effect of width on the properties of Faraday waves in hele-shaw cells, *Sci. China Phys. Mech. Astron.* **62**, 974711 (2019).
- [6] J. L. Gao, X. Z. Ma, G. H. Dong, H. Z. Chen, Q. Liu, and J. Zang, Investigation on the effects of Bragg reflection on harbor oscillations, *Coastal Eng.* **170**, 103977 (2021).
- [7] J. L. Gao, H. B. Shi, J. Zang, and Y. Y. Liu, Mechanism analysis on the mitigation of harbor resonance by periodic undulating topography, *Ocean Eng.* **281**, 114923 (2023).
- [8] D. J. Benney, Non-linear gravity wave interactions, *J. Fluid Mech.* **14**, 577 (1962).
- [9] M. S. Longuet-Higgins, Resonant interactions between two trains of gravity waves, *J. Fluid Mech.* **12**, 321 (1962).
- [10] F. P. Bretherton, Resonant interactions between waves. The case of discrete oscillations, *J. Fluid Mech.* **20**, 457 (1964).
- [11] F. Wen, Resonant generation of internal waves on the soft sea bed by a surface water wave, *Phys. Fluids* **7**, 1915 (1995).
- [12] M.-R. Alam, A new triad resonance between co-propagating surface and interfacial waves, *J. Fluid Mech.* **691**, 267 (2012).
- [13] W. Choi, M. Chabane, and T. M. A. Taklo, Two-dimensional resonant triad interactions in a two-layer system, *J. Fluid Mech.* **907**, A5 (2021).
- [14] S. J. Liao, On the homotopy multiple-variable method and its applications in the interactions of nonlinear gravity waves, *Commun. Nonlinear Sci. Numer. Simul.* **16**, 1274 (2011).
- [15] S. J. Liao, *Beyond Perturbation: Introduction to the Homotopy Analysis Method* (CRC Press, Boca Raton, FL, 2003).
- [16] S. J. Liao, *Homotopy Analysis Method in Nonlinear Differential Equations* (Springer-Verlag, New York, 2011).
- [17] D. L. Xu, Z. L. Lin, S. J. Liao, and M. Stiassnie, On the steady-state fully resonant progressive waves in water of finite depth, *J. Fluid Mech.* **710**, 379 (2012).
- [18] Z. Liu and S. J. Liao, Steady-state resonance of multiple wave interactions in deep water, *J. Fluid Mech.* **742**, 664 (2014).
- [19] Z. Liu, D. L. Xu, J. Li, T. Peng, A. Alsaedi, and S. J. Liao, On the existence of steady-state resonant waves in experiments, *J. Fluid Mech.* **763**, 1 (2015).
- [20] S. J. Liao, D. L. Xu, and M. Stiassnie, On the steady-state nearly resonant waves, *J. Fluid Mech.* **794**, 175 (2016).
- [21] Z. Liu, D. L. Xu, and S. J. Liao, Finite amplitude steady-state wave groups with multiple near resonances in deep water, *J. Fluid Mech.* **835**, 624 (2018).
- [22] Z. Liu and D. Xie, Finite-amplitude steady-state wave groups with multiple near-resonances in finite water depth, *J. Fluid Mech.* **867**, 348 (2019).
- [23] X. Y. Yang, F. Dias, Z. Liu, and S. J. Liao, Finite-amplitude steady-state resonant waves in a circular basin, *J. Fluid Mech.* **915**, A136 (2021).
- [24] E. Părău and F. Dias, Interfacial periodic waves of permanent form with free-surface boundary conditions, *J. Fluid Mech.* **437**, 325 (2001).
- [25] J. Y. Li, Z. Liu, S. J. Liao, and A. G. Borthwick, Steady-state harmonic resonance of periodic interfacial waves with free-surface boundary conditions based on the homotopy analysis method, *J. Fluid Mech.* **916**, A58 (2021).
- [26] J. Y. Li, Z. Liu, S. J. Liao, and A. G. Borthwick, Steady-state multiple near resonances of periodic interfacial waves with rigid boundary, *Phys. Fluids* **32**, 087104 (2020).
- [27] X. Y. Yang, F. Dias, and S. J. Liao, On the steady-state resonant acoustic-gravity waves, *J. Fluid Mech.* **849**, 111 (2018).
- [28] J. Li, Z. Liu, and J. Cui, Forces of fully nonlinear interfacial periodic waves on a cylindrical pile in a two-layer fluid with free-surface boundary conditions, *J. Ocean Eng. Sci.* **8**, 662 (2023).
- [29] J. Li, J. Cui, Z. Liu, X. Yang, and J. Zhou, On the steady-state interfacial waves with two-dimensional type—A double exact resonance, *Phys. Fluids* **36**, 012121 (2024).
- [30] T. M. Joyce, Nonlinear interactions among standing surface and internal gravity waves, *J. Fluid Mech.* **63**, 801 (1974).

- [31] J. E. Lewis, B. M. Lake, and D. R. S. Ko, On the interaction of internal waves and surface gravity waves, *J. Fluid Mech.* **63**, 773 (1974).
- [32] M. Tanaka and K. Wakayama, A numerical study on the energy transfer from surface waves to interfacial waves in a two-layer fluid system, *J. Fluid Mech.* **763**, 202 (2015).
- [33] S. A. Thorpe, On the shape of progressive internal waves, *Philos. Trans. R. Soc. London Ser. A* **263**, 563 (1968).